Zeitschrift für anorganische und allgemeine Chemie

Journal of Inorganic and General Chemistry
ZAAC
Zeitschrift für anorganische und allgemeine Chemie

RESEARCH ARTICLE OPEN ACCESS

Synthesis and Characterization of Anhydrous Cerium(III) Acetate, $[Ce(CH_3COO)_3]$, and its Interconversions to Hydrated Phases

Niklas Ruser[1] | Vanessa Behrens[1] | Christoph Meier[1] | Jennifer Theissen[2,3] | Felix Steinke[1] | Christian Näther[1] | Jonas Gosch[1] | Norbert Stock[1,4]

[1]Institute of Inorganic Chemistry, Kiel University, Kiel, Germany | [2]Centre for Membrane Separations, Adsorption Catalysis and Spectroscopy (cMACS), KU Leuven, Leuven, Belgium | [3]Institute for Materials Research (IMO-IMOMEC), Analytical and Circular Chemistry (ACC), NMR group, Hasselt University, Diepenbeek, Belgium | [4]Kiel Nano Surface and Interface Science (KiNSIS), Kiel University, Kiel, Germany

Correspondence: Norbert Stock (stock@ac.uni-kiel.de)

Received: 23 January 2026 | **Revised:** 2 April 2026 | **Accepted:** 4 May 2026

Keywords: cerium | coordination network | in situ | phase transformations | solvothermal synthesis

ABSTRACT

We report the synthesis and crystal structure of anhydrous cerium(III) acetate $[Ce(CH_3COO)_3]$ (**1**) as well as the interconversions to different hydrated phases. The structure determination of **1** was achieved by Rietveld refinement against powder X-ray diffraction (PXRD). Additionally, the thermal properties of **1** were investigated by thermogravimetry (TG) and variable-temperature PXRD (VT-PXRD) and a complete characterization was performed. **1** was prepared by solvothermal treatment of the sesquihydrate $[Ce_2(CH_3COO)_6(H_2O)_2]\cdot H_2O$ (**3**). The dehydration is reversible and **1** can be transformed back to **3**. Using VT-PXRD the transformation of **3** to **1** was studied. The step-wise dehydration does not proceed through $[Ce(CH_3COO)_3(H_2O)]$ **(2)**, instead another hitherto unknown metastable cerium(III) acetate hydrate (**4**) was observed. It was only possible to determine a sum formula of $Ce_2(CH_3COO)_6(H_2O)_2$ for **4**.

1 | Introduction

Metal acetates are important precursors for the synthesis of metal oxides [1–3] and metal–organic frameworks (MOFs) [4, 5]. Metal oxides [6, 7] and MOFs [8–10] derived from redox-active metals show catalytic properties, but in addition, the porous nature of MOFs also makes them suitable for gas adsorption [11, 12]. Many metals have been utilized to prepare metal oxides and MOFs, with lanthanide-containing compounds being particularly well-known for their luminescent properties [13, 14] and their use in organic synthesis [15]. Thus, numerous lanthanide acetates have been reported in the literature, containing, for example, La [16–18], Ce [18], Pr [19–21], Nd [18, 22, 23], Sm [23–26], Eu [18, 19, 23, 26–29], Gd [23, 26, 30, 31], Tb [24, 32], Dy [33], Ho [26, 34, 35], Er [26, 32, 35], Tm [36], Yb [26, 37] and Lu [18, 38]. These include both anhydrous and hydrated forms, as well as acetic acid solvates (Table S1). Many of these compounds have been obtained from an aqueous solution of the corresponding metal acetate by evaporation of water [18].

Among the lanthanides, cerium is of particular interest for applications in catalysis due to its redox chemistry [8, 9, 39–44]. Cerium(III) acetates were first mentioned by Maksimov et al. in 1957 [45] and Grigor'ev et al. [46] in 1964, who reported the synthesis of cerium(III) acetate sesquihydrate and cerium(III) acetate anhydrate. In 1968, Edwards et al. [47] reported the synthesis of anhydrous cerium(III) acetate by treatment of a commercial cerium(III) acetate hydrate in acetic acid/acetic anhydride under reflux and its characterization by elemental analysis (EA), thermogravimetry (TG) and infrared (IR) spectroscopy, but no PXRD data were presented. Anhydrous cerium(III) acetate was also reported in 2001 and 2002 by Arii et al. [48, 49] as an intermediate in a thermogravimetric study of commercial hydrated cerium(III)

acetate. In 1969, Karraker [50] was able to confirm the level of hydration of the sesquihydrate and the anhydrate, and rudimentary XRD data, that is, *d*-spacings were also reported. By combining results from IR and absorption spectroscopy, he was able to propose structural details for the sesquihydrate as Ce being eight- or nine-fold coordinated and the acetate anions acting as bridging and chelating ligands. For the anhydrous cerium(III) acetate, a coordination number of ≥9 for the Ce^{3+} ions and bridging acetate anions were postulated. Limited data on the crystal structures are available for the cerium(III) acetate hydrates. Thus unit cell parameters were published by Kvapil et al. [51] in 1973 and Meyer et al. [17] in 1993 for the cerium(III) acetate sesquihydrate and anhydrate, respectively, but no crystal structure refinement of the anhydrate was provided. The crystal structures of the monohydrate $[Ce(CH_3COO)_3(H_2O)]$ [18, 52] (**2**) and the sesquihydrate $[Ce_2(CH_3COO)_6(H_2O)_2]\cdot H_2O$ [18] (**3**) were published by Sadikov et al. [52] in 1968 and Junk et al. [18] in 1999, but the monohydrate was only characterized at room temperature. Single crystals of these compounds were obtained by evaporation of aqueous solutions of cerium(III) acetate, but no additional information on the characterization or even confirmation of bulk phase purity of these products was reported.

Summarizing, to the best of our knowledge, no systematic investigation concerning the synthesis, phase purity, and interconversion of the three known Ce(III) acetates has been reported. In this work we describe the synthesis and crystal structure of $[Ce(CH_3COO)_3]$ (**1**) and the reversible structural transformation from $[Ce_2(CH_3COO)_6(H_2O)_2]\cdot H_2O$ (**3**). Also, a new monohydrate $Ce_2(CH_3COO)_6(H_2O)_2$ (**4**) was observed. These studies were carried out by varying the temperature or the relative humidity (RH). In addition, characterization using PXRD, TG, EA, and IR spectroscopy was performed and the crystal structure of $[Ce(CH_3COO)_3(H_2O)]$ (**2**) was determined at low temperatures.

2 | Results and Discussion

The syntheses of three cerium acetates were accomplished using various synthetic routes ranging from solvothermal reactions, treatment at different temperatures and under saturated water vapor. Starting from commercially available $[Ce_2(CH_3COO)_6(H_2O)_2]\cdot H_2O$ (**3**), solvothermal treatment in acetonitrile at 150°C for 2 h resulted in the formation of the fully dehydrated product $[Ce(CH_3COO)_3]$ (**1**). The treatment of **1** in an atmosphere saturated with water vapor resulted in the recrystallization of **3**. In addition, a fourth crystalline product with the sum formula of $Ce_2(CH_3COO)_6(H_2O)_2$ (**4**) was observed during the thermal treatment of **3** in air, before **1** has formed as the final product. These structural transformations will be discussed in detail below. Additionally, the crystal structure of **2** has been determined at 100 K and is presented in the Supporting Information (Section S4).

2.1 | Crystal Structure Determination

Analysis of a PXRD pattern of **1** using Topas Academic [53] suggested several possible unit cell parameters and space groups. These results were used to search for isostructural compounds in the Cambridge Structural Database (CSD) [54] using ConQuest [55]. The trigonal space group $R\bar{3}$ (No. 148) with a, $b = 21.88$ Å and $c = 9.85$ Å resulted in $[La(CH_3COO)_3]$ (Refcode: PEWJUW [17]) as a possible match. Therefore, this crystal structure was used as the starting structural model and was refined against PXRD data using the Rietveld algorithm [56] in Topas Academic [53] (Figure 1). Hence, La was replaced by Ce, and the bond lengths and angles of the acetate ions were refined using z-matrices. Individual temperature factors were used for Ce and the atoms of each acetate ion, respectively. For the peak fit, the Thompson-Cox-Hastings-pseudo-Voigt function was used. The background was modeled using strongly broadened reflections from an hkl-phase. The crystallographic data are shown in Table S2.

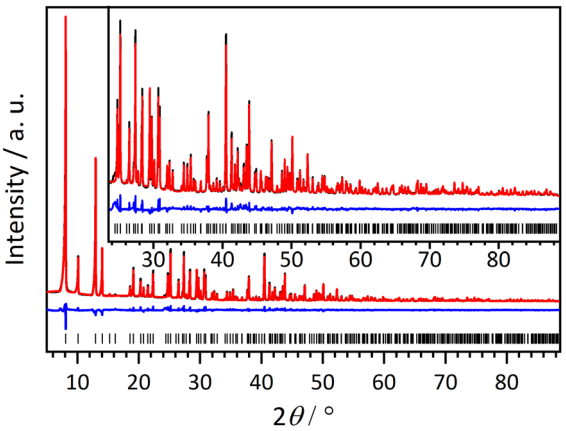

FIGURE 1 | Final Rietveld plot of the structure refinement of **1** with the measured PXRD pattern (black), the calculated PXRD pattern (red), the resulting difference (blue) and allowed reflection positions (black ticks).

2.2 | Crystal Structures

The crystal structure of **1** is shown in Figure 2. The cerium cations are tenfold coordinated by oxygen atoms all originating from acetate anions (Figure 2a). The asymmetric unit contains one cerium cation and three acetate anions (Figure 2b). Each cerium cation is coordinated by eight acetate ions, six of them coordinate in the monodentate mode, and two are chelating (Figure 2c). The refined Ce–O distances, ranging from 2.446(7) to 2.720(9) Å, are in good agreement with values of other cerium compounds retrieved from the CSD [54] analyzed with the help of the software ConQuest [55] and Mercury [57].

The connection of the cerium cations by the acetate anions leads to edge- and face-sharing CeO_{10} polyhedra, which results in a three-dimensional inorganic building unit (IBU). The IBU exhibits a complex connectivity. However, subdividing it into hexamers facilitates the structural description of the IBU. In each hexamer, the CeO_{10} polyhedra are connected via common edges within the *ab*-plane, while along the *c*-axis face-sharing CeO_{10} polyhedra are found (Figure 2d). Each hexamer is connected to two other hexamers, forming a ladder-like arrangement that proceeds along the *c*-axis (Figure 2e). These ladders are further connected to two neighboring ladders through O atoms (edge-sharing CeO_{10} polyhedra), forming hexagonal tubes that contain potential voids along the *c*-axis (Figure 2f), which are occupied by the methyl groups of the acetate ions. These tubes are connected via common edges (Figures 2g and S3) and form a honeycomb-like structure (Figure 2h).

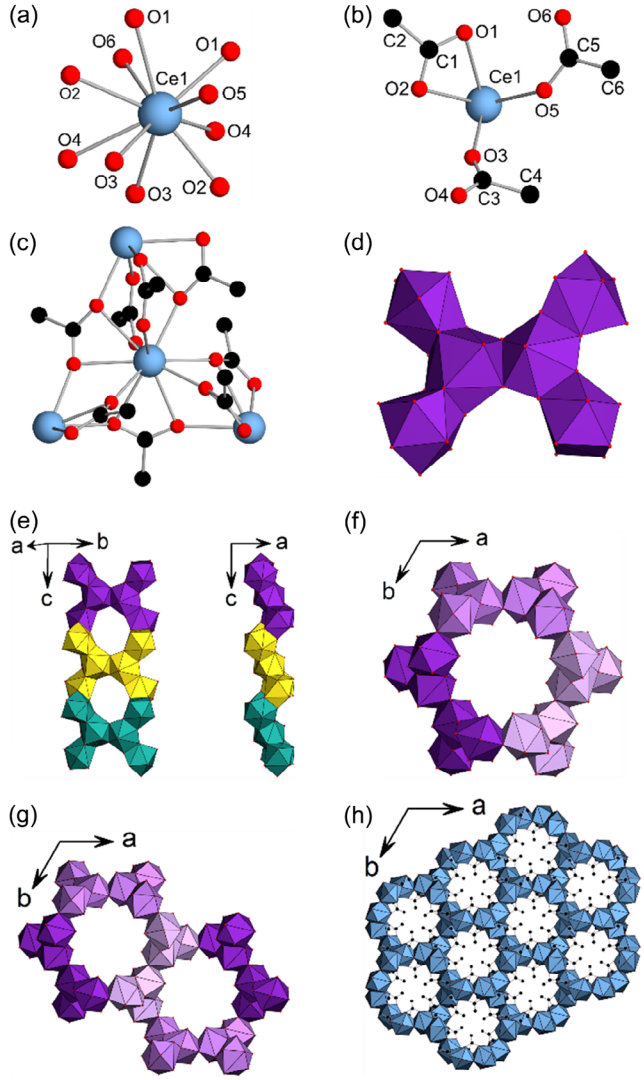

FIGURE 2 | Representation of the crystal structure of **1**. (a) Coordination environment of the cerium cations. (b) Asymmetric unit of the crystal structure. (c) Connection of the cerium cations by the acetate anions. (d) Hexamer composed of CeO_{10} polyhedra. (e) Ladder-like arrangement by connection of one hexamer to two adjacent hexamers (purple, yellow and green are used for better distinguishability). (f,g) Pores made up by interconnection of ladders (different shades of purple are used to distinguish the different ladders). (h) Honeycomb framework observed in **1** with methyl groups pointing into the pores. CeO_{10}-polyhedra are colored differently (except for blue) to improve the distinction of the hexamers.

The crystal structure of **2** was redetermined at 100 K by single-crystal X-ray diffraction (SCXRD) from a single crystal found in an aged batch of commercial cerium(III) acetate sesquihydrate. Structural details of **2** are presented in Section S4.

2.3 | Thermal Properties of 1

Compound **1** was characterized regarding its thermal properties, phase changes, decomposition temperature, and thermal expansion by TG and VT-PXRD. According to the TG data **1** exhibits a thermal stability up to 180°C (Figure S8) and the sum formula of $[Ce(CH_3COO)_3]$ could be confirmed (Section S5). In contrast, the VT-PXRD experiment (Figure S10) of **1** showed a loss of long-range order at approx. 260°C. This temperature difference is due to different measurement conditions.

2.4 | Phase Transformations

The phase transformations were studied by heat treatment of the samples (TG and VT-PXRD) or exposure to water vapor at high RH values. An overview of the observed phase transformations can be found in Figure 3.

Anhydrous cerium(III) acetate (**1**) is accessible through a solvothermal treatment of **3** (see experimental section). To study the reversibility of the dehydration of **3**, an in situ PXRD measurement of **1** was carried out under well-defined RH values up to 80% RH, the maximum achievable value for the set-up (Figure S12). Up to 80% RH, only compound **1** is present. To study the influence of higher RH values and longer exposure time **1** was stored at 100% RH and 20°C for 88 h and was analyzed ex situ (Figure 4). According to PXRD, compound **1** completely transformed to **3** under these conditions. The transformation during the dehydration of **3** was also

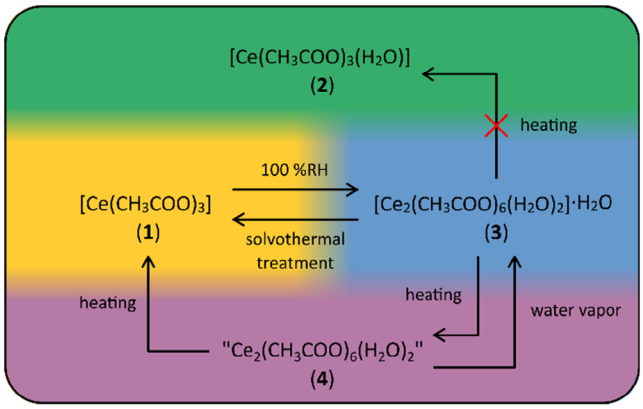

FIGURE 3 | Overview of the conditions that lead to the phase transformations between the cerium(III) acetates. Compound **4** could only be obtained as a metastable product and the crystal structure could not be determined. Compound **2** was not observed in the systematic study.

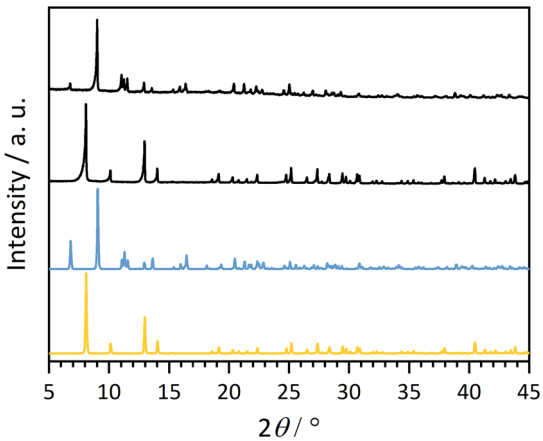

FIGURE 4 | Comparison of the calculated PXRD patterns of **1** (yellow) and **3** [18] (blue) with the measured PXRD patterns of **1** before (black, bottom) and after 88 h under 100% RH at 20°C (black, top).

studied in situ by VT-PXRD, and the data are shown in Figure 5. In this context it is noted that the data show the presence of another crystalline compound at the beginning of the experiment. This phase crystallized prior to the measurement from a pure sample of **3** upon aging (Section S6.2 and Figure S13). While no information about the transformation leading to this phase mixture could be gained, it was used to study the temperature-dependent phase transformations. At low temperatures ranging between 25 and 70°C, the reflection intensities of **3** decrease continuously with increasing temperature, while the intensities of the additional reflections increased in the same temperature range. At 85°C, no reflections indicating the presence of **1**, **2,** or **3** are observed, indicating phase purity of the crystalline phase (**4**) at this temperature. Further heating to 100–175°C yielded an X-ray amorphous product, and between 175 and 190°C compound, **1** started to crystallize and remained stable up to 205°C. Between 205 and 220°C, **1** began to lose its long-range order. The final product of this experiment is CeO_2 (Figure S14).

Additional experiments were carried out to synthesize and characterize product **4** that was observed in situ during the VT-PXRD study. It was found that heating **3** at 115°C for 1 h in a ventilation oven leads to the formation of **4** (Figure 6). The elevated temperatures indicate that the loss of water molecules of **3** leads to the formation of **4**. This is also confirmed by the results of the TG measurements of **3** and **4** (Figure 7). In the TG curve of **3**, two distinct mass losses between 26 and 109°C and 109 and 186°C are observed, corresponding to the loss of approximately one and two water molecules per sum formula, respectively, while the TG curve of **4** shows only one distinct weight loss between 109 and 181°C. These findings indicate **4** being another cerium(III) acetate hydrate with a sum formula of $Ce_2(CH_3COO)_6(H_2O)_2$ (Tables S3 and S4). It is noted that this compound is formally also a monohydrate as **2**. However, the PXRD patterns are substantially different as shown in Figure 6. The different temperatures needed for obtaining **4** by VT-PXRD (85°C), TG (109°C) and the temperature treatment in an oven (115°C) likely arise due to the different experimental conditions including the heating rate, different ambient relative humidity values and volumes of the sample holders. Unfortunately, no crystals suitable for SCXRD could be obtained and indexing of the PXRD pattern of **4** was unsuccessful, so that no crystal structure could be retrieved. Under ambient conditions (24.4°C, 40% RH) **4** transforms partially back into compound **3** within minutes (Figure S16). Still, additional reflections are observed that change with time, which could not be assigned to the known phases. Further details are given in Section S7.

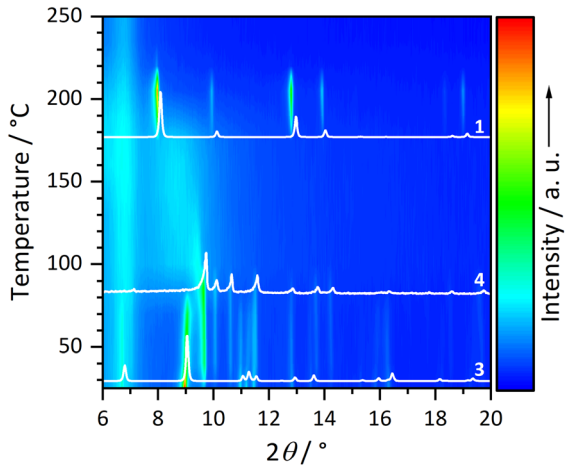

FIGURE 5 | Variable-temperature PXRD (VT-PXRD) measurement of a mixture of **3** and **4** in comparison with the calculated PXRD patterns of **1**, **3** [18] and the measured PXRD pattern of **4**.

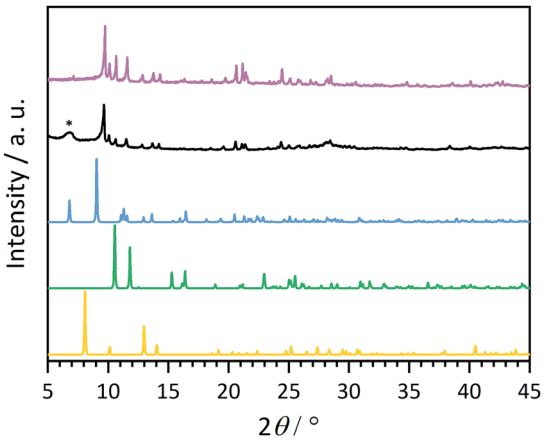

FIGURE 6 | Comparison of the calculated PXRD patterns of **1** (yellow), **2** [18] (green) and **3** [18] (blue) with the measured PXRD patterns of **3** from the VT-PXRD measurement at 85°C (black) and after treatment at 115°C for 1 h (purple). The marked reflection (*) is an artifact caused by the heating chamber.

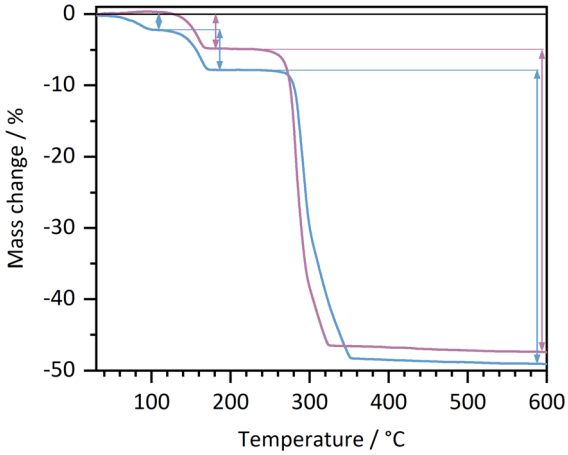

FIGURE 7 | TG curves of **3** (blue) and **4** (purple) measured with a heating rate of 8 K/min under constant air flow (6 L/h).

3 | Conclusion

We presented a systematic study on the transformation of cerium(III) acetates, demonstrating the impact of temperature and relative humidity on the product composition. The cerium(III) acetate anhydrate $[Ce(CH_3COO)_3]$ (**1**) and sesquihydrate $[Ce_2(CH_3COO)_6(H_2O)_2]\cdot H_2O$ (**3**) can be easily transformed into each other at high relative humidity or by thermal treatment, respectively. The full characterization including the crystal structure of **1**, is reported for the first time. The structure determination was successfully carried out by Rietveld refinement against PXRD data. **1** exhibits a three-dimensional IBU made up of edge- and face-

sharing CeO_{10} polyhedra. As confirmed by TG and VT-PXRD measurements, **1** shows a moderate thermal stability in the temperature range of 30–180°C. Under relative humidity of 0–80% for 20 min, **1** remains stable. Exposing **1** to 100% RH for 88 h, the formation of **3** was observed. Dehydration of **3** under air and elevated temperatures also led to **1**, as shown by VT-PXRD. Surprisingly, the transformation of **3** to **1** does not proceed through the formation of **2**, but a new product with the sum formula $Ce_2(CH_3COO)_6(H_2O)_2$ (**4**) that is formed as an intermediate. Our systematic investigation shows that in addition to the previously known cerium(III) acetates, one new metastable phase was found. Also, in the supposedly simple cerium(III) acetate hydrate system some hydration/dehydration processes can be easily performed (**1**↔**3**) while others (**1**→**2** or **3**→**2**) cannot be achieved. Thus, the reproducible formation of **2** is still an open scientific question. Additionally, the crystal structure of **2** was determined at 100 K.

4 | Experimental Section

All used chemicals were used without further purification. $Ce(CH_3COO)_3{\cdot}xH_2O$ was obtained from TCI (>98%). It was identified as phase pure **3** by PXRD and IR spectroscopy (Figures S1 and S2, respectively). Acetonitrile (≥99.9%) was purchased from Honeywell.

Microwave-assisted syntheses were carried out in a Biotage Initiator+ synthesizer. TG measurements were performed on a Linseis STA PT 1600 with a heating rate of 8 K/min and constant air flow (6 L/h) with the samples being located in open Al_2O_3 crucibles. EA was carried out on an Elementar vario MICRO cube. For IR spectroscopy a Bruker ALPHA-P ATR MIR spectrometer was employed.

Powder X-ray diffraction (PXRD) measurements were conducted on a STOE Stadi P instrument equipped with a DECTRIS MYTHEN2 1K detector using Cu $K_{\alpha1}$ ($\lambda = 1.540598$ Å) radiation. The VT-PXRD measurement of **1** was conducted on the same STOE Stadi P diffractometer using a STOE capillary furnace, with the sample being located in an open quartz capillary with a diameter of 0.5 mm and a wall thickness of 0.01 mm. One PXRD pattern was collected at 30°C as the starting point and consecutive PXRD patterns were collected in the range of 40–600°C with steps of 20°C for 39 min per PXRD pattern for **1**. A heating ramp of 50°C/min between the targeted temperatures was applied. Since the PXRD patterns showed pronounced background modulations, the background was subtracted with the Raw Data Handling module within the WinXPOW software (Version 3.10) from STOE & Cie GmbH for visual representation of the data. The refinement of the cell parameters was carried out using the raw data. The VT-PXRD measurement of **3** was performed using a Malvern Panalytical Empyrean diffractometer equipped with an Anton Paar TTK 600 chamber, a nonmonochromated Cu radiation (Cu $K_{\alpha1}$ = 1.540598 Å, Cu $K_{\alpha2}$ = 1.544426 Å) and a PIXcel 3D 1x1 solid-state pixel detector. The diffraction experiments were performed in Bragg–Brentano configuration using a 0.02 rad Soller slit on both the incident and diffracted beam sides, and a ¼° divergence slit on the incident beam. The sample was mounted on a flat sample holder with an integrated heating element and positioned to ensure optimal alignment with the incident X-ray beam. The diffractometer was configured to scan over a 2θ range from 5° to 50°, with a fixed step size of 0.0263° per measurement point. The exposure time was set to 10 s/step. The first PXRD pattern was collected at 25°C, with consecutive PXRD patterns being measured in an interval of 15°C up to 400°C under synthetic air. The sample was heated at a rate of 10°C/min, with an equilibration period of 15 min at each target temperature before data collection. Each PXRD pattern was collected for 45 min. Variable relative-humidity PXRD measurements were performed at the BM26 beamline at the European Synchrotron Radiation Facility (ESRF, Grenoble, France), using an incident beam with an energy of 12 keV ($\lambda = 1.03320$ Å). The humidity conditions were controlled using a gas dosing system equipped with four mass flow controllers (MFCs) to create N_2/H_2O mixtures at relative humidities ranging from 10% to 80%. At each humidity setting, an equilibration period of 10 min was allowed before data collection. For each measurement, multiple PXRD patterns were accumulated over a total measurement time of ≈20 min, and the resulting summed diffractogram is presented. SCXRD was performed with a XtaLAB Synergy, Dualflex, HyPix diffractometer from Rigaku using Cu-K_α radiation.

4.1 | Synthesis of $[Ce(CH_3COO)_3]$ (1)

367.2 mg (0.5333 mmol) of **3** were transferred into an 11 mL glass vial. 4 mL acetonitrile as well as a magnetic stirring bar were added and the vial was sealed. The synthesis was carried out by microwave-assisted heating at a temperature of 150°C for 2 h and a stirring rate of 300 rpm. After cooling to room temperature, the white precipitate was filtered off and washed three times with 2 mL acetonitrile. After drying under air, the product was obtained as a white microcrystalline powder. EA (meas./calc.): C/wt% = (22.54/22.72), H/wt% = (2.90/2.86), N/wt% = (0.26/0.00). Yield: 329.3 mg (1.038 mmol, 97.28%). An IR spectrum of **1** was collected and the data is presented in Figure S2.

4.2 | Synthesis of $[Ce_2(CH_3COO)_6(H_2O)_2]{\cdot}H_2O$ (3)

30.0 mg (0.0945 mmol) of **1** was ground thoroughly and exposed to a saturated water atmosphere by placing it into a desiccator over an excess amount of demineralized water. Thus, an atmosphere with a RH of 100% was established and the sample was left under these conditions for 88 h at 20°C. Afterwards, the product was dried in air for 30 min at ambient conditions.

4.3 | Synthesis of 4

30.0 mg (0.0435 mmol) of **3** were heated in a glass vial at 115°C for 1 h in a preheated oven with forced ventilation under air. The sample was immediately characterized since it is unstable under ambient conditions and starts to rehydrate to **3** immediately at 24.4°C and 40% RH. For collecting the reference PXRD pattern, the sample was prepared in scotch tape without delay after the synthesis to isolate it from air humidity. This sealing was enough to prevent a transformation within the measurement time of 30 min.

Author Contributions

Niklas Ruser: conceptualization, investigation, validation, formal analysis, visualization, writing – original draft, writing – review and editing.

Vanessa Behrens: validation, formal analysis. **Christoph Meier**: validation, formal analysis. **Jennifer Theissen**: investigation, formal analysis, writing – review and editing. **Felix Steinke**: formal analysis. **Christian Näther**: investigation, formal analysis, writing – review and editing. **Jonas Gosch**: investigation. **Norbert Stock**: conceptualization, supervision, funding acquisition, project administration, writing – original draft, writing – review and editing.

Acknowledgments

The authors thank the spectroscopic division of the department of inorganic chemistry at Kiel University for the conducted IR and EA measurements. The authors would like to thank Martin Rosenthal for assistance and support in using beamline BM26 at ESRF. Bastian Achenbach is acknowledged for contributing helpful ideas on this topic.

Open Access funding enabled and organized by Projekt DEAL.

Funding

The authors thank the state of Schleswig-Holstein for the financial support. N.R., J.G., and N.S. acknowledge the support by the Deutsche Forschungsgemeinschaft (STO-643/15−1). J.T. acknowledges the support by the FWO and F.R.S.-FNRS (Belgium) under the Excellence of Science (EOS) program ('PHOSPORE' – EOS reference number: 40,007,504). We acknowledge the European Synchrotron Radiation Facility (ESRF) for the provision of synchrotron radiation facilities under proposal number A26-2-999.

Conflicts of Interest

The authors declare no conflicts of interest.

Data Availability Statement

Data available on request from the authors. The full crystallographic data has been deposited in the Cambridge Crystallographic Data Centre (CCDC) under the deposition numbers CCDC 2524105 and 2524110 for **1** and **2**, respectively. This data can be obtained free of charge.

References

1. R. V. Kumar, Y. Diamant, and A. Gedanken, "Sonochemical Synthesis and Characterization of Nanometer-Size Transition Metal Oxides From Metal Acetates," *Chemistry of Materials : A Publication of the American Chemical Society* 12 (2000): 2301–2305.

2. R. Sui, P. A. Charpentier, and R. A. Marriott, "Synthesizing 1D and 2D Metal Oxide Nanostructures: Using Metal Acetate Complexes as Building Blocks," *Nanoscale* 12 (2020): 17971–17981.

3. E. Marceau, M. Che, J. Čejka, and A. Zukal, "Nickel(II) Nitrate vs. Acetate: Influence of the Precursor on the Structure and Reducibility of Ni/MCM-41 and Ni/Al-MCM-41 Catalysts," *ChemCatChem* 2 (2010): 413–422.

4. G. Lee and J. Hwang, "Direct Synthesis of Mixed-Metal Paddle-Wheel Metal–Organic Frameworks with Controlled Metal Ratios Under Ambient Conditions," *Inorganic Chemistry* 62 (2023): 19457–19465.

5. M. Richezzi, P. R. Donnarumma, C. Copeman, and A. J. Howarth, "Rare-Earth Acetates as Alternative Precursors for Rare-Earth Cluster-Based Metal–organic Frameworks," *Chem. Commun* 60 (2024): 5173–5176.

6. Y. Li, Y. Zhang, K. Qian, and W. Huang, "Metal–Support Interactions in Metal/Oxide Catalysts and Oxide–Metal Interactions in Oxide/Metal Inverse Catalysts," *Acs Catalysis* 12 (2022): 1268–1287.

7. J. C. Védrine, "Metal Oxides in Heterogeneous Oxidation Catalysis: State of the Art and Challenges for a More Sustainable World," *ChemSusChem* 12 (2019): 577–588.

8. S. Smolders, J. Jacobsen, N. Stock, and D. de Vos, "Selective Catalytic Reduction of NO by Cerium-Based Metal–organic Frameworks," *Catalysis Science & Technology* 10 (2020): 337–341.

9. S. Smolders, K. A. Lomachenko, B. Bueken, et al., "Unravelling the Redox-catalytic Behavior of Ce^{4+} Metal–Organic Frameworks by X-ray Absorption Spectroscopy," *Chemphyschem: A European Journal of Chemical Physics and Physical Chemistry* 19 (2018): 373–378.

10. A. Bavykina, N. Kolobov, I. S. Khan, J. A. Bau, A. Ramirez, and J. Gascon, "Metal–Organic Frameworks in Heterogeneous Catalysis: Recent Progress, New Trends, and Future Perspectives," *Chemical Reviews* 120 (2020): 8468–8535.

11. X. Wu, Z. Bao, B. Yuan, et al., "Microwave Synthesis and Characterization of MOF-74 (M=Ni, Mg) for Gas Separation," *Microporous Mesoporous Mater* 180 (2013): 114–122.

12. C. A. Trickett, A. Helal, B. A. Al-Maythalony, Z. H. Yamani, K. E. Cordova, and O. M. Yaghi, "The Chemistry of Metal–organic Frameworks for CO2 Capture, Regeneration and Conversion," *Nature Reviews Materials* 2 (2017): 17045.

13. J.-C. G. Bünzli and C. Piguet, "Taking Advantage of Luminescent Lanthanide Ions," *Chemical Society Reviews* 34 (2005): 1048–1077.

14. O. Guillou, C. Daiguebonne, G. Calvez, and K. Bernot," A Long Journey in Lanthanide Chemistry: From Fundamental Crystallogenesis Studies to Commercial Anticounterfeiting Taggants," *Accounts of Chemical Research* 49 (2016): 844–856.

15. G. A. Molander, "Application of Lanthanide Reagents in Organic Synthesis," *Chemical Reviews* 92 (1992): 29–68.

16. M. T. Weller, P. F. Henry, V. P. Ting, and C. C. Wilson, "Crystallography of Hydrogen-Containing Compounds: Realizing the Potential of Neutron Powder Diffraction," *Chemical Communications* 21 (2009): 2973–2989.

17. G. Meyer and D. Gieseke-Vollmer, "Das Wasserfreie Lanthanacetat, $La(CH_3COO)_3$, Und Sein Precursor, $NH_4)_3$ $[La(CH_3COO)_6]$ · 1/2 H_2O: Synthese, Strukturen, Thermisches Verhalten," *Zeitschrift Fur Anorganische Und Allgemeine Chemie* 619 (1993): 1603–1608.

18. P. C. Junk, C. J. Kepert, L. Wei-Min, B. W. Skelton, and A. H. White, "Structural Systematics of Rare Earth Complexes. X ('Maximally') Hydrated Rare Earth Acetates," *Australian Journal of Chemistry* 52 (1999): 437–458.

19. S. Ganapathy, V. P. Chacko, R. G. Bryant, and M. C. Etter, "Carbon CP-Mass NMR and X-Ray Crystal Structure of Paramagnetic Lanthanide Acetates," *Journal of the American Chemical Society* 108 (1986): 3159–3165.

20. A. Lossin and G. Meyer, "Praseodym (III) acetat-sesquihydrat, Pr (CH3COO) 3l, 5H20,"*Zeitschrift Fur Naturforschung. Teil B* 47 (1992): 1602–1608.

21. A. Lossin and G. Meyer, "$Pr(CH_3COO)_3$, Ein Wasserfreies Selten-Erd-Acetat Mit Netzwerkstruktur," *Zeitschrift Fur Anorganische Und Allgemeine Chemie* 620 (1994): 438–443.

22. S. Gomez Torres and G. Meyer, "Anhydrous Neodymium(III) Acetate," *Zeitschrift Fur Anorganische Und Allgemeine Chemie* 634 (2008): 231–233.

23. M. Haase, P. Rissiek, M. Gather-Steckhan, F. Henkel, and H. Reuter, "Structural Evolution in the RE(OAc)3 · 2AcOH Structure Type. A Non-Linear, One-Dimensional Coordination Polymer with Unequal Interatomic Rare Earth Distances," *Crystals* 11 (2021): 768.

24. Q. Yu, X. Zhou, M. Liu, et al., "Syntheses, Characterization, and Luminescence of Two Lanthanide Complexes [Ln2(acetate)6(H2O) 4]·4H2O (Ln=Tb(1), Sm(2))," *J. Rare Earths* 26 (2008): 178–184.

25. A. Lossin, G. Meyer, R. Fuchs, and J. Strähle, "[Sm $(CH_3COO)_3(H_2O)$ 2]· CH3COOH, ein Essigsäureaddukt des Samarium (III)-acetatdihydrate," *Zeitschrift Fur Naturforschung. Teil B* 47 (1992): 179–182.

26. R. Vaďura and J. Kvapil, "Growth and Lattice Parameters of the Lanthanide Carboxylates I. Tetrahydrated Lanthanide Acetates," *Materials Research Bulletin* 6 (1971): 865–873.

27. P. Starynowicz, "Structure and Spectroscopy of Diaqua(μ3-Acetato)(acetato-O)(acetic Acid-O)europium(II), [Eu(OAc)2(AcOH)(H2O)2]," *Polyhedron* 14 (1995): 3573–3577.

28. P. Starynowicz, "Synthesis and Crystal Structure of Europium(II) Diacetate Hemihydrate, Eu(CH3COO)2·0.5H2O," *Journal of Alloys and Compounds* 268 (1998): 47–49.

29. S. Gomez Torres, I. Pantenburg, and G. Meyer, "Direct Oxidation of Europium Metal with Acetic Acid: Anhydrous Europium(III) Acetate, $Eu(OAc)_3$, Its Sesqui-hydrate, $Eu(OAc)_3(H_2O)_{1.5}$, and the "Hydrogen-diacetate", $[Eu(H(OAc)_2)_3](H_2O)$," *Zeitschrift Fur Anorganische Und Allgemeine Chemie* 632 (2006): 1989–1994.

30. F.-S. Guo, J.-D. Leng, J.-L. Liu, Z.-S. Meng, and M.-L. Tong, "Polynuclear and Polymeric Gadolinium Acetate Derivatives with Large Magnetocaloric Effect," *Inorganic Chemistry* 51 (2012): 405–413.

31. L. Cañadillas-Delgado, O. Fabelo, J. Cano, et al., "Dinuclear and Two- and Three-Dimensional Gadolinium(III) Complexes with Mono- and Dicarboxylate Ligands: Synthesis, Structure and Magnetic Properties," *CrystEngComm* 11 (2009): 2131–2142.

32. Y. Zhu, Y. Tao, C. Yang, et al., "Breaking Symmetry for SHG Response: Lanthanide Acetate Crystals via Water Molecule Regulation Strategy," *Inorganic Chemistry* 63 (2024): 21230–21237.

33. R. Baggio, J. C. Muñoz, and M. Perec, "Bis (μ-acetato-κ3O, O′: O′) bis [bis (acetato-κ2O, O′) diaquadysprosium (III)] tetrahydrate," *Acta Crystallographica* C58 (2002): m498–m500.

34. J. Janczak and R. Kubiak, "Reactivity of the HoPc2I in the Acetylacetone–water System," *Polyhedron* 81 (2014): 695–704.

35. A. M. Pauls, D. U. Jamadgni, G. George, J. N. Gitua, and M. M. Thuo, "Stereo-Structural Fine Tuning of Chromaticity," *Angewandte Chemie International Edition* 63 (2024): e202318949.

36. I. G. Fomina, M. A. Kiskin, A. G. Martynov, et al., "Lanthanum (III), Samarium (III), Europium (III), and Thulium (III) binuclear acetates and pivalates: Synthesis, structure, magnetic properties, and solid-phase thermolysis," *Zhurnal Neorganicheskoi Khimii* 49 (2004): 1463–1474.

37. R. A. Zehnder, R. A. Renn, and F. R. Fronczek, "Acetato-κ2O, O′) dihydroxidoytterbium (III) Hemihydrate," *Acta Crystallographica* C66 (2010): m307–m310.

38. A. Lossin and G. Meyer, "Wasserfreie Selten-Erd-Acetate, $M(CH_3COO)_3$ (M = Sm–Lu, Y) Mit Kettenstruktur. Kristallstrukturen von $Lu(CH_3COO)_3$ Und $Ho(CH_3COO)_3$," *Zeitschrift Fur Anorganische Und Allgemeine Chemie* 619 (1993): 1609–1615.

39. D. Morelli Venturi, M. Sole Notari, L. Trovarelli, et al., "Synthesis, Structure and (Photo)Catalytic Behavior of Ce-MOFs Containing Perfluoroalkylcarboxylate Linkers: Experimental and Theoretical Insights," *Chemistry – A European Journal* 30 (2024): e202400433.

40. J. Lyu, X. Zhang, P. Li, et al., "Exploring the Role of Hexanuclear Clusters as Lewis Acidic Sites in Isostructural Metal–Organic Frameworks," *Chemistry of Materials: A Publication of the American Chemical Society* 31 (2019): 4166–4172.

41. R. Dalapati, B. Sakthivel, A. Dhakshinamoorthy, et al., "A Highly Stable Dimethyl-Functionalized Ce(Iv)-Based UiO-66 Metal–organic Framework Material for Gas Sorption and Redox Catalysis," *CrystEngComm* 18 (2016): 7855–7864.

42. M. Campanelli, T. Del Giacco, F. de Angelis, et al., "Solvent-Free Synthetic Route for Cerium(IV) Metal–Organic Frameworks with UiO-66 Architecture and Their Photocatalytic Applications," *Acs Applied Materials & Interfaces* 11 (2019): 45031–45037.

43. C. Xu and X. Qu, "Cerium Oxide Nanoparticle: A Remarkably Versatile Rare Earth Nanomaterial for Biological Applications," *Npg Asia Materials* 6 (2014): e90.

44. T. Montini, M. Melchionna, M. Monai, and P. Fornasiero, "Fundamentals and Catalytic Applications of CeO_2-Based Materials," *Chemical Reviews* 116 (2016): 5987–6041.

45. V. N. Maksimov, A. V. Novoselova, and K. N. Semenenko, "OB ATSETATE LANTANA," *Zhurnal Neorganicheskoi Khimii* 2 (1957): 997.

46. A. J. Grigor'ev and V. N. Maksimov, "Infrared Absorption Spectra of Acetates of Group Iii of The Periodic Table and of Their Hydrates," *Zhurnal Neorganicheskoi Khimii* 9 (1964): 1060.

47. D. A. Edwards and R. N. Hayward, "Transition Metal Acetates," *Canadian Journal of Chemistry* 46 (1968): 3443–3446.

48. T. Arii, A. Kishi, M. Ogawa, and Y. Sawada, "Thermal Decomposition of Cerium(III) Acetate Hydrate by a Three-Dimensional Thermal Analysis," *Analytical Sciences: the International Journal of the Japan Society for Analytical Chemistry* 17 (2001): 875–880.

49. T. Arii, T. Taguchi, A. Kishi, M. Ogawa, and Y. Sawada, "Thermal Decomposition of Cerium(III) Acetate Studied with Sample-Controlled Thermogravimetric–mass Spectrometry (SCTG—MS)," *Journal of the European Ceramic Society* 22 (2002): 2283–2289.

50. D. G. Karraker, "Coordination of Lanthanide Acetates," *Journal of Inorganic and Nuclear Chemistry* 31 (1969): 2815–2832.

51. J. Kvapil and R. Vaďura, "Growth and Lattice Parameters of the Lanthanide Carboxylates II. Sesquihydrated Lanthanide Acetates," *Materials Research Bulletin* 8 (1973): 807–812.

52. G. G. Sadikov, G. A. Kukina, and M. A. Porai-Koshits, "X-Ray Structure of Cerium Triacetate Hydrate," *Journal of Structural Chemistry* 8 (1968): 492–493.

53. A. A. Coelho, "*TOPAS* and *TOPAS-Academic*: an Optimization Program Integrating Computer Algebra and Crystallographic Objects Written in C++," *Journal of Applied Crystallography* 51 (2018): 210–218.

54. C. R. Groom, I. J. Bruno, M. P. Lightfoot, and S. C. Ward, "The Cambridge Structural Database," *Acta Crystallographica* B72 (2016): 171–179.

55. I. J. Bruno, J. C. Cole, P. R. Edgington, et al.,"New Software for Searching the Cambridge Structural Database and Visualizing Crystal Structures," *Acta Crystallographica* B58 (2002): 389–397.

56. H. M. Rietveld, "Line Profiles of Neutron Powder-Diffraction Peaks for Structure Refinement," *Acta Crystallographica* 22 (1967): 151–152.

57. C. F. Macrae, I. Sovago, S. J. Cottrell, et al., "*Mercury 4.0*: From Visualization to Analysis, Design and Prediction," *Journal of Applied Crystallography* 53 (2020): 226–235.

Supporting Information

Additional supporting information can be found online in the Supporting Information section.